

# ADVANCED MATERIALS

## Supporting Information

for *Adv. Mater.*, DOI: 10.1002/adma.202007682

Translocation of DNA through Ultrathin Nanoslits

*Wayne Yang, Boya Radha, Adnan Choudhary, Yi You,  
Gangaiah Mettela, Andre K. Geim, Aleksei Aksimentiev,\*  
Ashok Keerthi,\* and Cees Dekker\**

# Supplementary information

## Translocation of DNA through ultrathin nanoslits

Wayne Yang<sup>1</sup>, Boya Radha<sup>2,3</sup>, Adnan Choudhary<sup>4</sup>, Gangaiah Mettela<sup>2</sup>, Yi You<sup>2,3</sup>,  
Andre Geim<sup>2,3</sup>, Aleksei Aksimentiev<sup>4\*</sup>, Ashok Keerthi<sup>3,5\*</sup>, Cees Dekker<sup>1\*</sup>

\*Correspondence: aksiment@illinois.edu, ashok.keerthi@manchester.ac.uk, c.dekker@tudelft.nl

<sup>1</sup>Kavli Institute of Nanoscience Delft, Delft University of Technology, The Netherlands

<sup>2</sup>Department of Physics & Astronomy, School of Natural Sciences, University of Manchester, Oxford Road, Manchester M13 9PL, United Kingdom.

<sup>3</sup>National Graphene Institute, University of Manchester, Manchester M13 9PL, UK

<sup>4</sup>Department of Physics, Beckman Institute for Advanced Science and Technology, University of Illinois at Urbana-Champaign, Urbana, IL, USA.

<sup>5</sup>Department of Chemistry, School of Natural Sciences, University of Manchester, Oxford Road, Manchester M13 9PL, United Kingdom.

### Table of Contents

<b><i>S1 Fabrication of 2D nanoslit devices .....</i></b>	<b><i>2</i></b>
<b><i>S2 AFM profile of a 2D nanoslit.....</i></b>	<b><i>5</i></b>
<b><i>S3 Mounting and wetting procedure for the 2D nanoslit .....</i></b>	<b><i>6</i></b>
<b><i>S4 Additional sample events of DNA translocation in 2D nanoslit .....</i></b>	<b><i>7</i></b>
<b><i>S5 DNA translocation in hBN 2D nanoslit .....</i></b>	<b><i>8</i></b>
<b><i>S6 MD simulation setup.....</i></b>	<b><i>9</i></b>
<b><i>S7 Additional current trace of DNA events obtained from coarsed grained simulations ...</i></b>	<b><i>11</i></b>
<b><i>S8 Histogram of current blockade and characterisation of event types .....</i></b>	<b><i>12</i></b>

## S1 Fabrication of 2D nanoslit devices

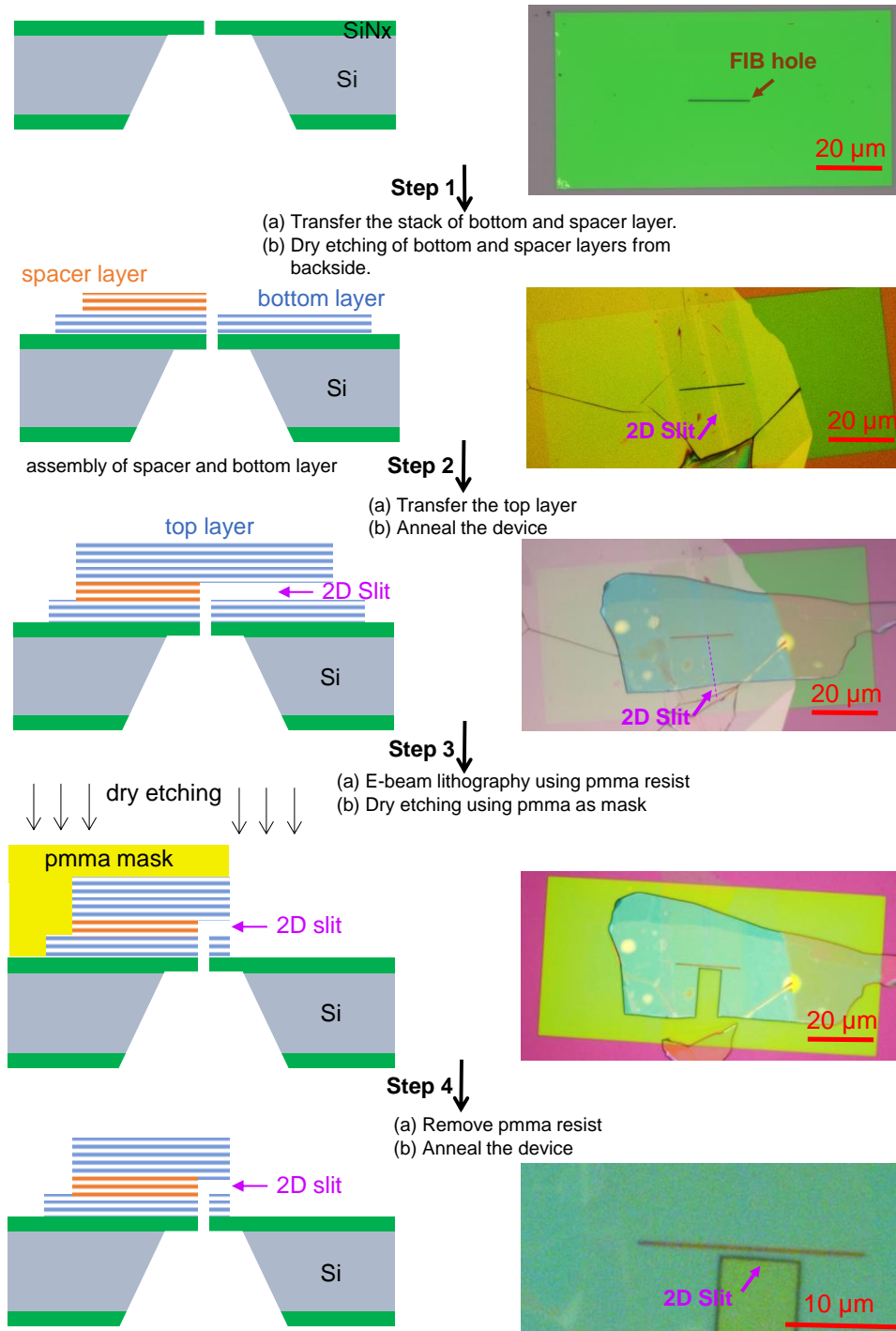


**Figure S1. Device fabrication flow chart.**

Fabrication of 2D nanoslit devices is illustrated in Fig. S1. The fabrication procedure was originally reported in Keerthi *et al*<sup>1</sup> and modified for our single channel device.

Preparation of SiN membrane: We prepared a free-standing silicon nitride ( $\text{SiN}_x$ ) membrane with dimensions of about  $50 \mu\text{m} \times 100 \mu\text{m}$  using photolithography and wet etching, starting with a standard silicon (Si) wafer covered with 500 nm-thick layer of  $\text{SiN}_x$  on both sides. A narrow rectangular hole ( $\sim 300 \text{ nm} \times 20 \mu\text{m}$ ) was drilled by focused ion beam (FIB) on the free-standing  $\text{SiN}_x$  membrane which is pre-coated with  $\sim 10 \text{ nm}$  aluminium on both sides of the membrane. Aluminium coating helped to alleviate the charging of the insulating  $\text{SiN}_x$  membrane. After drilling the hole, the aluminium was removed by treating the  $\text{SiN}_x$  wafer with alkaline solution (Microposit® MF319 developer). Following this, the membranes were exposed to oxygen plasma for  $\sim 3$  mins to clean the surface.

Patterning and etching of graphene slit: In the next step, a mechanically exfoliated thin ( $\sim 5$  to  $6.5 \text{ nm}$ , error  $\sim 0.1 \text{ nm}$ ) crystals of graphite were prepared on an oxidized Si wafer ( $300 \text{ nm}$  of  $\text{SiO}_2$ ). These crystals were then patterned and etched to make one long slit of  $110 \text{ nm}$  width. Extra nanocavities were created perpendicular to the main 2D-slit to prevent the formation of contamination bubbles formed from collected hydrocarbon contaminants during the self-cleansing process that happens when two 2D-crystals are placed on top of each other, as reported previously<sup>2</sup>. These cavities were perpendicular to the main channel and did not contribute to DNA translocation through the final devices. Patterning was done by electron-beam lithography using polymethyl methacrylate (PMMA) as a resist and oxygen plasma to etch away graphite. The PMMA mask was removed by mild sonication in acetone. The resulting patterned spacer crystal were transferred on to a bottom layer (around  $\sim 20\text{-}30 \text{ nm}$  thick graphite or hexagonal boron nitride, h-BN) on another oxidized Si wafer.

Transfer of graphene stack: The double layer stack of bottom and spacer layers was transferred together by a wet transfer method, onto the previously made FIB milled aperture on the  $\text{SiN}_x$  membrane as shown in Fig. S1- Step1a. Following the transfer, the hole was extended into this stack by dry etching from the underside of the  $\text{SiN}_x/\text{Si}$  wafer (Fig. S1- Step1b). To this end, dry etching with oxygen plasma was used for graphite, whereas h-BN was etched in a mixture of  $\text{CHF}_3$  and oxygen.

Sealing of graphene slits: In the next step, a relatively thick ( $\sim 150 \text{ nm}$ ) crystal of h-BN/graphite was chosen as the top layer. For the case of graphite 2D slits, the top graphite crystal was covered with another hBN crystal ( $\sim 50 \text{ nm}$  thick) which will later be used as a mask for a later etching step. The top layer was precisely transferred on top of the bottom and spacer stack so that it covers the FIB rectangular aperture and overlapped with the 2D-slit (Fig. S1- Step2a). After each transfer, the substrate was annealed in 10% hydrogen-in-argon at  $400 \text{ }^\circ\text{C}$  for  $5 \text{ h}$ . The annealing steps are essential for the cleanliness of the final devices and to avoid the clogging 2D slits with PMMA residues and other contaminants from the fabrication processes.

Defining the length of the channel: To define the desired length (L) of the 2D-slit in the final device, we used another step of e-beam lithography. After the pattern writing, the PMMA was used as mask to etch away top and bottom layers using dry-etching methods (Fig. S1- Step3). In the case of graphite 2D-slit devices, first, hBN present on the top graphite layer was etched, and using this hBN as a mask, graphite layers of remaining top, spacer and bottom crystals were etched. After etching, the PMMA was removed by dry etching. The final devices were annealed at 400 °C for 5 hrs (Fig. S1- Step4) and stored in DI water.

## S2 AFM profile of a 2D nanoslit

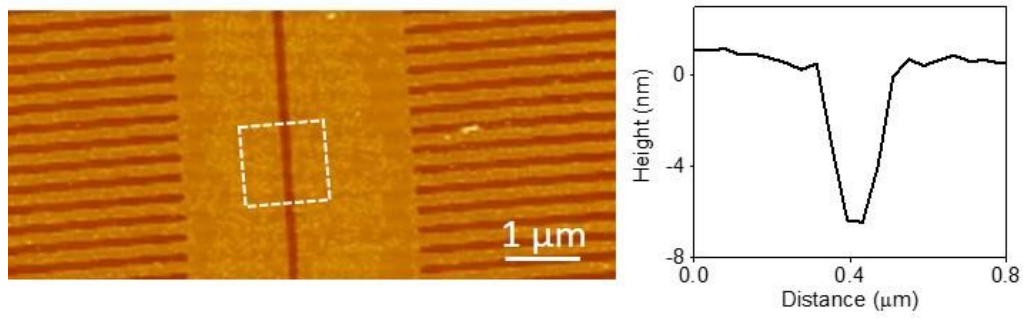


**Figure S2.** AFM line profile of nanoslit. An AFM line profile across an open 2D nanoslit device (before the top layer is transferred), showing the low ( $< 1$  nm) RMS roughness. The height profile is taken from the area shown in the dotted white box. The perpendicular nanocavities for the collection of contaminants can be seen in the image.

### S3 Mounting and wetting procedure for the 2D nanoslit

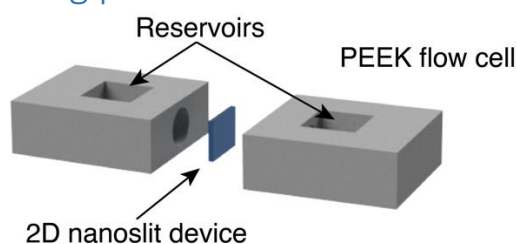


**Figure S3.** Schematic of PEEK flow cell used to mount 2D nanoslit. The 2D nanoslit device was mounted in a PEEK flow cell containing two large reservoirs ( $\sim 500\mu\text{l}$  in volume). For the wetting procedure, the following order was used. First, the device was rinsed with EtOH and gently blow-dried with a  $\text{N}_2$  gun. The device was then mounted into the PEEK flowcell. To help with the wetting of the 2D nanoslit, the following order of solution were used. First, the reservoirs were filled with 100% Ethanol. The Ethanol solution was then replaced by a solution containing 50% Ethanol and 50% MiliQ. That solution was then replaced by MiliQ several times (2-3 times) to ensure that all ethanol was removed from the reservoirs in order to prevent precipitation of DNA. Finally, the MiliQ was replaced by the desired salt solution (1,2,4 M LiCl). An Ag/AgCl electrode was inserted into each of the reservoir and connected to an Axopatch 200B amplifier (Molecular Devices) and the conductance of the slit was measured. The entire wetting procedure was repeated until the device obtained the expected conductance for the given geometry of the fabricated 2D nanoslit.

## S4 Additional sample events of DNA translocation in 2D nanoslit

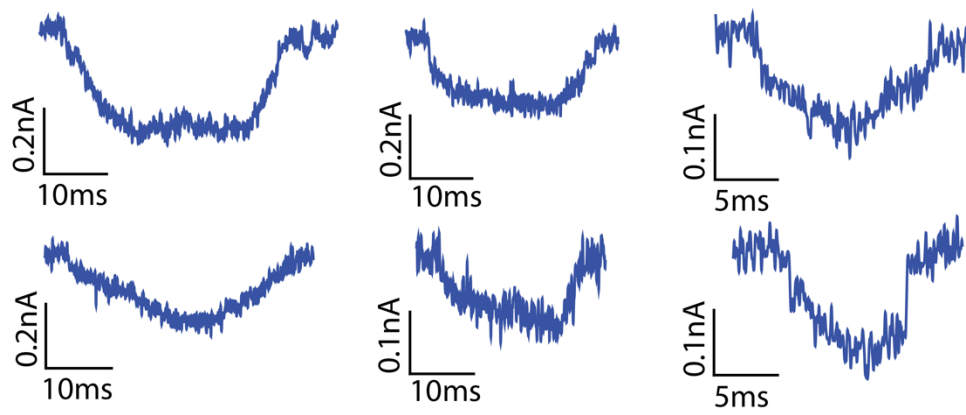


**Figure S4.** Additional DNA translocation event from the experiments in (300mV, 4M LiCl).

## S5 DNA translocation in hBN 2D nanoslit

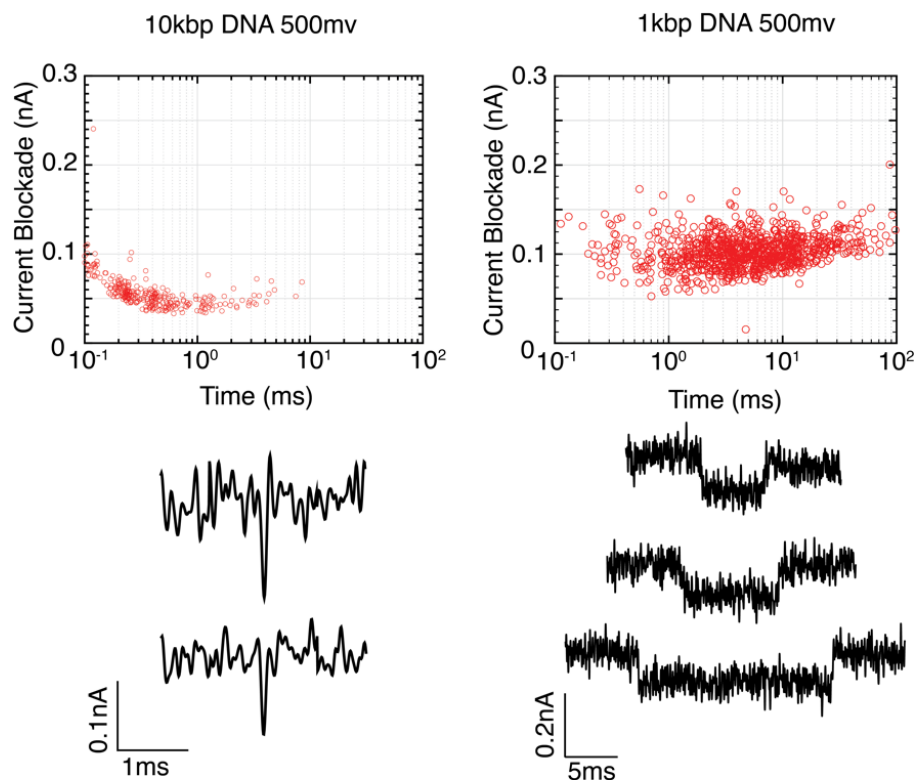


**Figure S5.** hBN 2D-nanoslit device with DNA translocation events. We observed exclusively spike events for the 10kbp DNA experiment while the experiment with 1kbp showed primarily DNA translocation event marked by higher current blockade and longer dwell time of the event.

A hBN nanoslit device ( $1 \mu\text{m} \times 6\text{nm} \times 116\text{nm}$ ) was fabricated using the procedure outlined in S1 with hBN top and bottom stacks used instead of graphene. Similar to the wetting procedure outline above, the slit was mounted in a PEEK flow cell and buffered with 2M LiCl. An I-V curve was taken to ensure that the device was properly wetted prior to the addition of 10 kbp DNA on the cis side of the flow cell at a bias voltage of 500mV. Similar to the data reported in the main paper, We observe only probing events characterised by short and quick spikes (left column of figure). The device was thoroughly cleaned by rinsing with buffer solution, EtOH and water repeatedly before dismounting. The device was stored in MiliQ water for several days to rinse out any remaining DNA material. The device was then annealed at  $250 \text{ }^\circ\text{C}$  in air for 2 hours to ensure complete degradation of DNA and drying of the slit. The device was then remounted and wetted with 2 M LiCl, of which the conductance remained the same as the first experiments with 10kbp DNA. Then 1kbp DNA was introduced from the cis side (+500mV). This time, clear DNA translocation can be seen showing up as longer blockade in the current trace as well as longer translocation times as seen from the collected scatter plot on the right (right column of figure).

## S6 MD simulation setup

All simulations of dsDNA translocation through the nanoslit were performed using the Atomic Resolution Brownian Dynamics (ARBD) package<sup>3</sup>. COMSOL software (COMSOL Multiphysics 5.3a) was used to obtain the electrostatic potential that was applied in ARBD. This process is described in detail below.

**Continuum modeling.** The COMSOL software package was used to generate continuum solutions to the electrostatics problem. The computational domain consists of a  $160 \text{ nm}^3$  initial reservoir, a  $400 \times 110 \times 3.5 \text{ nm}^3$  slit that emerges from the center of the face of the initial reservoir and connects seamlessly to the top face of a  $160 \text{ nm}^3$  final reservoir. The material properties of the interior of the system were set to those of water, *i.e.*,  $100 \text{ kg/m}^3$  density,  $0.00089 \text{ Pa}\cdot\text{s}$  dynamic viscosity, and a relative permittivity of 80. The distribution of the electrostatic potential was obtained using the Electrostatics module. The external potential was introduced into the calculation as Dirichlet boundary conditions on the  $x$ -face opposite the slit in the initial reservoir and the  $z$ -face opposite the slit in the final reservoir. We used a two-step process to obtain the mesh upon which COMSOL solved the Laplace's equation. First, a free tetrahedral mesh was created using a predefined 'Extremely fine' element size everywhere. We used the resulting mesh to find the initial solution to the electrostatics problem. Next, the solution was refined 5 times using an adaptive mesh procedure with a maximum coarsening factor and element growth rate of 3. The resulting mesh was then saved and used to solve all the electrostatics problems in this work.

**MD simulations.** All simulations were performed using a GPU-accelerated simulation engine ARBD, a 40 fs simulation time step, and a two-bead-per-basepair model of dsDNA that was previously described<sup>4</sup>. The central bead in this model represents the interaction sites within double-stranded segments while the orientation bead represents the local twist of the helix. The bonded interactions in this model are enforced through harmonic potentials, while the non-bonded interactions were chosen to match the experimental measurements of Rau and Parsegian for DNA in a 25 mM  $\text{MgCl}_2$  electrolyte<sup>5</sup>. A Langevin integration scheme was used to maintain a constant temperature with diffusion constants of 120 and  $79 \text{ \AA}^2/\text{ns}$  for the central and orientation beads, respectively. The CG MD simulation of ssDNA was coupled to the electrostatic potentials extracted from a continuum COMSOL model in the form of an external grid-based potential that applied to the central beads of the DNA. Each central bead was assigned an effective charge of  $0.5e$ , where  $e$  is the charge of an electron, to account for electroosmotic forces<sup>6,7</sup>. Additionally, a repulsive steric potential was applied, in the form of a 3D grid potential, to prevent the DNA from penetrating the solid boundaries of the system. The steric potential was generated using the `find_boundaries` routine of the `image`

processing Python module, scikit-image<sup>8</sup>, to identify a set of boundary layers (in steps matching the 1 nm × 1 nm × 0.5 nm resolution of the grid) from the binary geometry data exported from COMSOL. The values of the steric potential were zero in the reservoirs and slits and increased with each boundary layers as  $kd^2$  where  $k=100$  kcal/mol and  $d$  is the distance in nanometers outside the solid boundaries of the system. Our coarse-grained simulations used point particle beads to represent DNA base pairs. The height that the beads could explore in our simulations was set to 3.5 nm, Figure S6. Physically, this corresponded to a slit height of about 6nm when the full diameter of DNA is taken into account, which is about the same height as the slit reported in the experiments. The length and width of the simulated slit was 400 and 110 nm, respectively. Prior to translocation simulations, a 5000-bp DNA strand was equilibrated in a 160 nm<sup>3</sup> volume using a multi-resolution simulation protocol. The initial conformation of the molecule was a straight line extending from (0,-55,-80) nm to (0,55,80) nm. The system was equilibrated in five steps of increasing resolution. We started with 10<sup>8</sup> steps of duration 200 fs/step with a resolution of 100 bp/bead. We then moved on to 10<sup>7</sup> steps at 200 fs/step with 50 bp/bead, 10<sup>7</sup> steps at 200 fs/step with 25 bp/bead, 10<sup>7</sup> steps at 100 fs/step with 5 bp/bead, and finally 2×10<sup>6</sup> steps at 40 fs/step with 1 bp/bead. Eighteen DNA conformations were created in this manner and used to initiate the 18 translocation simulations performed.

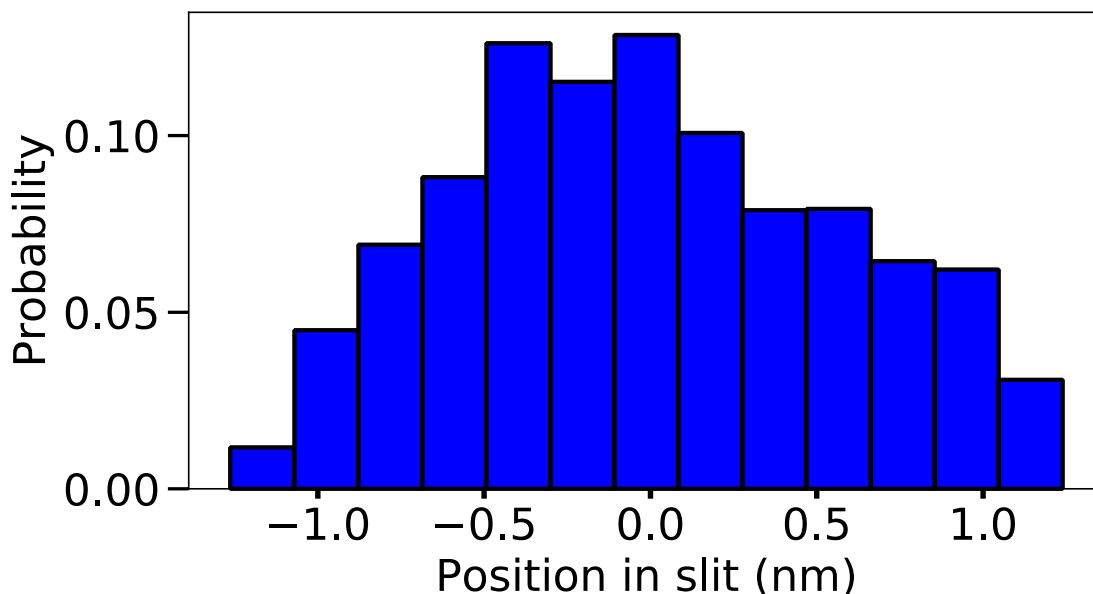


**Figure S6.** Distribution of the vertical (normal to the slit plane) coordinate of the ~2500 (central) beads representing the molecule of DNA. The 3.5 nm height of the slit accessible to the DNA beads corresponds to an experimental slit height of 5.7 nm, taking into account the 2.2 nm diameter of the DNA.

## S7 Additional current trace of DNA events obtained from coarsened simulations

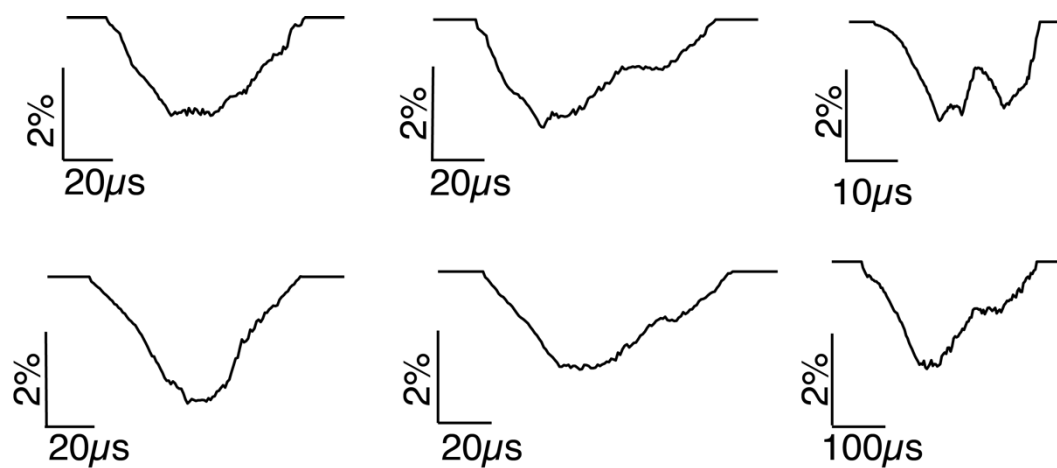


**Figure S7:** Simulated current trace of DNA events obtained from coarse-grained Brownian dynamics simulations.

## S8 Histogram of current blockade and characterisation of event types

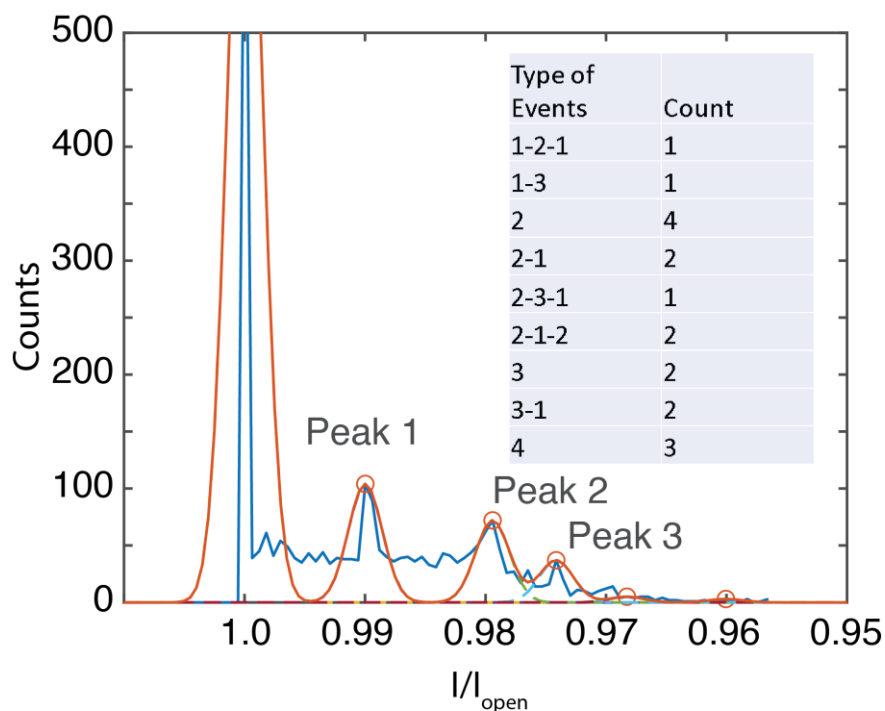


**Figure S8:** Histogram of the current blockade level achieved for all 16 simulation runs and characterisation of event types. We can identify clear peaks arising from the plateaus from the simulated current trace. We sorted the event type by the plateau levels that they achieved during the translocation process (i.e., peak 1 = type 1). Matching the simulations, we see that the event type corresponds to the number of folds or loops in DNA present in the slit. We did not see a pure type1-only translocation in the simulations which would correspond to a single helix of ds-DNA translocating through the slit. At higher numbers, the accuracy between the number of folds and strands of the DNA diverges because the DNA can adopt different configurations which produces the same number of equivalent DNA strands.

## References:

1. Keerthi, A. *et al.* Ballistic molecular transport through two-dimensional channels. *Nature* **558**, 420–424 (2018).
2. Haigh, S. J. *et al.* Cross-sectional imaging of individual layers and buried interfaces of graphene-based heterostructures and superlattices. *Nat. Mater.* **11**, 764–767 (2012).
3. Comer, J. & Aksimentiev, A. Predicting the DNA Sequence Dependence of Nanopore Ion Current Using Atomic-Resolution Brownian Dynamics. *J. Phys. Chem. C* **116**, 3376–3393 (2012).
4. Maffeo, C. & Aksimentiev, A. MrDNA: a multi-resolution model for predicting the structure and dynamics of DNA systems. *Nucleic Acids Res.* **48**, 5135–5146 (2020).
5. Rau, D. C., Lee, B. & Parsegian, V. A. Measurement of the repulsive force between polyelectrolyte molecules in ionic solution: hydration forces between parallel DNA double helices. *Proc. Natl. Acad. Sci. U. S. A.* **81**, 2621–5 (1984).
6. Luan, B. & Aksimentiev, A. Electro-osmotic screening of the DNA charge in a nanopore. *Phys. Rev. E* **78**, 021912 (2008).
7. van Dorp, S., Keyser, U. F., Dekker, N. H., Dekker, C. & Lemay, S. G. Origin of the electrophoretic force on DNA in solid-state nanopores. *Nat. Phys.* **5**, 347–351 (2009).
8. van der Walt, S. *et al.* scikit-image: image processing in Python. *PeerJ* **2**, e453 (2014).